Materials Today: Proceedings 45 (2021) 5400–5404

Contents lists available at ScienceDirect

Materials Today: Proceedings

journal homepage: www.elsevier.com/locate/matpr

Analysis of mechanical properties between submerged and normal multiple-pass friction stir processing of the FSWed dissimilar aluminium joints

Sipokazi Mabuwa *, Velaphi Msomi

Cape Peninsula University of Technology, Mechanical Engineering Department, Bellville 7535, South Africa

A R T I C L E I N F O

Article history:
Available online 26 February 2021

Keywords:
Hardness
Microstructure
Tensile properties
Rapid cooling
Dynamic recrystallization

A B S T R A C T

The friction stir welded dissimilar aluminium alloy joints AA8011-AA6082 were subjected to multiple-pass friction stir processing under different operating conditions. The processing conditions used included room temperature (normal) and underwater (submerged) friction stir processing. Microstructural analysis, hardness and tensile tests were conducted to analyze the impact of different multiple-pass friction stir processing conditions on the friction stir welded dissimilar aluminium alloy joints. The microstructural results showed that the multiple-pass submerged friction stir processed grain structure was 67.72% finer compare to those of the multiple-pass normal friction stir processed joints. The ultimate tensile strength obtained correlated the grain size behaviour resulting in the multiple-pass submerged joint having a UTS with a 3.2% increase in comparison to that of the normal friction stir processed joints. The percentage elongation results correlated with the tensile and grain size results. The multiple-pass submerged friction stir processed joints had a maximum hardness of 65 HV and the normal multiple-pass friction stir processed joints had a hardness of 53 HV.

Second International Conference on Aspects of Materials Science and Engineering (ICAMSE 2021).

1. Introduction

Friction stir processing is the rising solid-state microstructural refinement technique originating from the friction stir welding technique [1–3]. The refinement of the microstructure is as a result of extensive plastic deformation and the heat caused by friction on the material during the processing leading to notable changes in the processed area [4]. The refined microstructure results in the improvement of the mechanical properties of the processed area [2]. Numerous studies have been conducted on the FSP of both similar and dissimilar aluminium alloy joints. FSP continues to grow and recently evolved to submerged friction stir processing (SFSP). The SFSP technique works similar to normal friction stir processing (NFSP) but differs on the processing medium which is the immersed environment. Both NFSP and SFSP have been successfully utilized in many applications. However, the application of multiple-pass friction stir processing was found to be very effective for further microstructural refinement [5–10].

It was noted that most studies available on literature reports mostly on the multiple–pass friction stir processing under normal conditions. There is little literature reporting on the multiple-pass friction stir processing under submerged conditions. Additionally, on the little literature available it was noted that the FSP of similar joints has more consideration and less attention is given to both NFSP and SFSP of dissimilar aluminium joints. In this study, the mechanical properties of the submerged and normal multiple-pass friction stir processed friction stir welded dissimilar aluminium alloy joints will be analyzed comparatively. The outcomes of this study will be of great help in the manufacturing applications of components for engineering industries especially automotive and industrial engineering.

2. Materials and methods

The considered materials in this study were the AA6082 and AA8011. Table 1 shows the chemical composition of the materials determined by the energy-dispersive X-ray spectroscopy machine. The dimensions of the plates used were 250 × 55 × 6 mm. The dissimilar plates were fabricated using the friction stir welding technique utilizing the converted semi-automated milling machine.

* Corresponding author.
E-mail address: sipokazimabuwa@gmail.com (S. Mabuwa).

https://doi.org/10.1016/j.matpr.2021.02.101
2214-7853/
Second International Conference on Aspects of Materials Science and Engineering (ICAMSE 2021).

Table 1
Chemical compositions.

	Mg	Zn	Ti	Cr	Si	Mn	Fe	Cu	Al
AA8011-H14	0.28	0.084	0.016	0.028	0.52	0.46	0.74	0.13	Bal
AA6082-T6	0.6–1.2	0.0–0.2	0.0–0.10	0.0–0.20	0.7–1.3	0.0–1.0	0.0–0.5	0.0–0.1	Bal

Table 2
FSW/FSP parameters [11].

Rotational speed (rpm)	Traverse speed (mm/min)	Tool shoulder (mm)	Tilt angle	Tool probe diameter (mm)	Tool pin length	Dwell time (s)
1100	60	20	2°	7	5.8	10

Table 3
Mechanical properties [8,9,13].

	Ultimate tensile strength (MPa)	Percentage elongation (%)	Hardness (HV)	Mean grain size (μm)
AA6082	308	25.22	91.57	65.09
AA8011	94.1	39.98	33.8	51.68
NFSP: AA8011-AA6082	86.92	24.27	50.5	5.18
SFSP: AA8011-AA6082	90.19	25.32	55	3.22

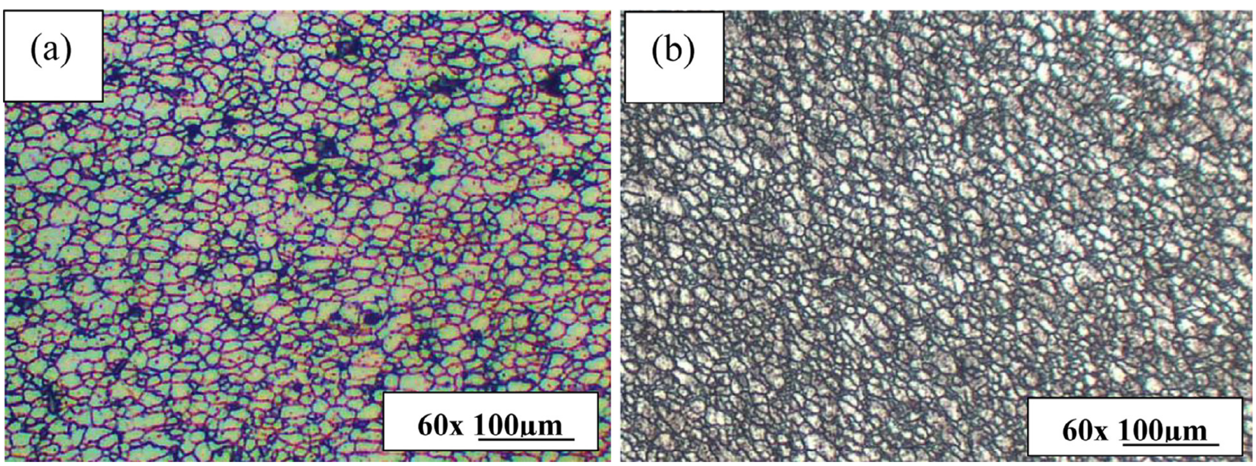

Fig. 1. Stir zone multiple-pass micrographs, (a) NFSP, (b) SFSP.

Table 2 show the welding parameters used for FSW. The high-speed steel material was used for the manufacturing of the tool used [11]. During both friction stir welding and processing the AA8011 plate was located on the advancing side, while on the AA6082 plate was on the retreating side. Post FSW the formed joints were friction stir processed using a total of four pass friction stir processing under normal and submerged FSP conditions. The friction stir welded (FSWed) and the friction stir processed multiple-pass plates were cut using the waterjet technology for different specimens concerning the tests conducted. The tests conducted include microstructure, tensile and hardness tests. The post-tensile specimens were further analyzed using the scanning electron microscopy (SEM) for the nature of the fracture.

The microstructure was conducted on the Motic AE2000 metallurgical microscope. The linear intercept method through ImageJ software was used to measure the grain size. The linear intercept method is detailed under ASTM E112-13. It works by drawing a number of equal lengths along a given sample with a known scale, identify the number of times each line intercept a new grain, add up a total number of intersections from all the lines drawn and divide the total length by the number of the intersections [12]. The specimens were etched using the Weck's reagent was applied first and followed by the modified Keller's reagent. The tensile tests were conducted using the Hounsfield 50 K tensile testing machine. The operating parameters and specimen geometry were abducted from the ASTM-E8M-04. The Tescan SEM equipment was used for SEM and the hardness was conducted using the falcon 500 hardness testing machine. The Vickers hardness test was performed using the ASTM E384-11. The 500 g load, 10 × and the 20 × objectives were used to focus the specimen. The interval of 1 mm was used. The mechanical properties of the FSW and 1 pass NSFP and SFSP properties are presented in Table 3.

3. Results and discussion

Fig. 1 shows the stir zone micrographs of the multiple-pass NFSP and SFSP joints. The multiple-pass NFSP joint was found to have the average gain size of 2.93 μm with a standard deviation of 2.03 μm, while the multiple-pass SFSP joint had an average grain size of 1.21 μm and a standard deviation of 1.65 μm. The multiple-pass SFSPed joints had finer grains compared to that of the multiple NFSP joints. This is due to the reduction of grain growth as a result of the processing medium where the processed region experiences enhanced rapid cooling rate [13–15]. Additionally, the

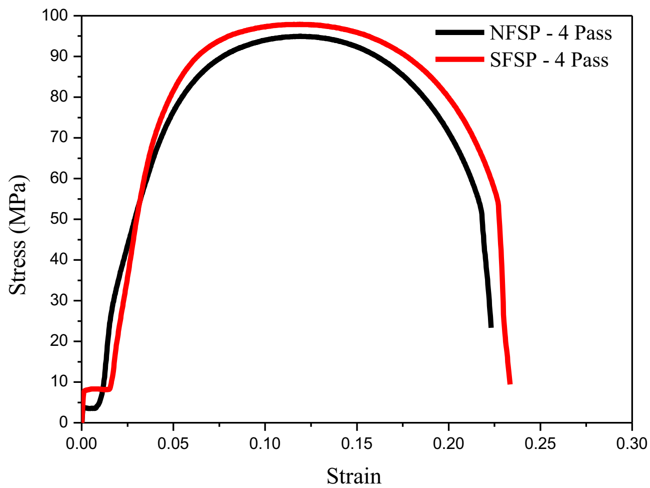

Fig. 2. Tensile stress and strain curves.

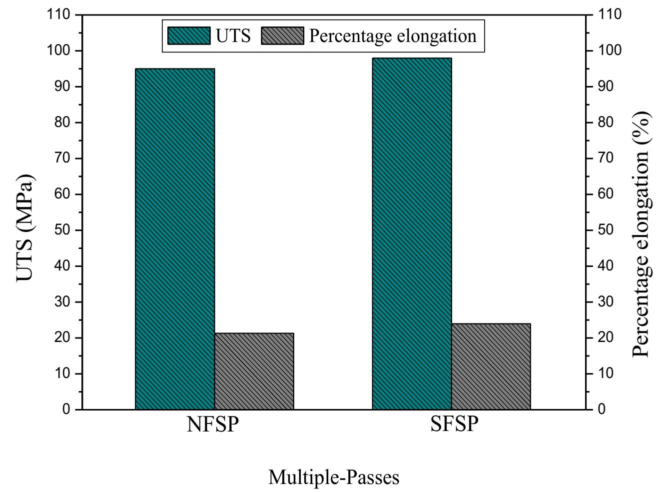

Fig. 3. UTS and percentage elongation.

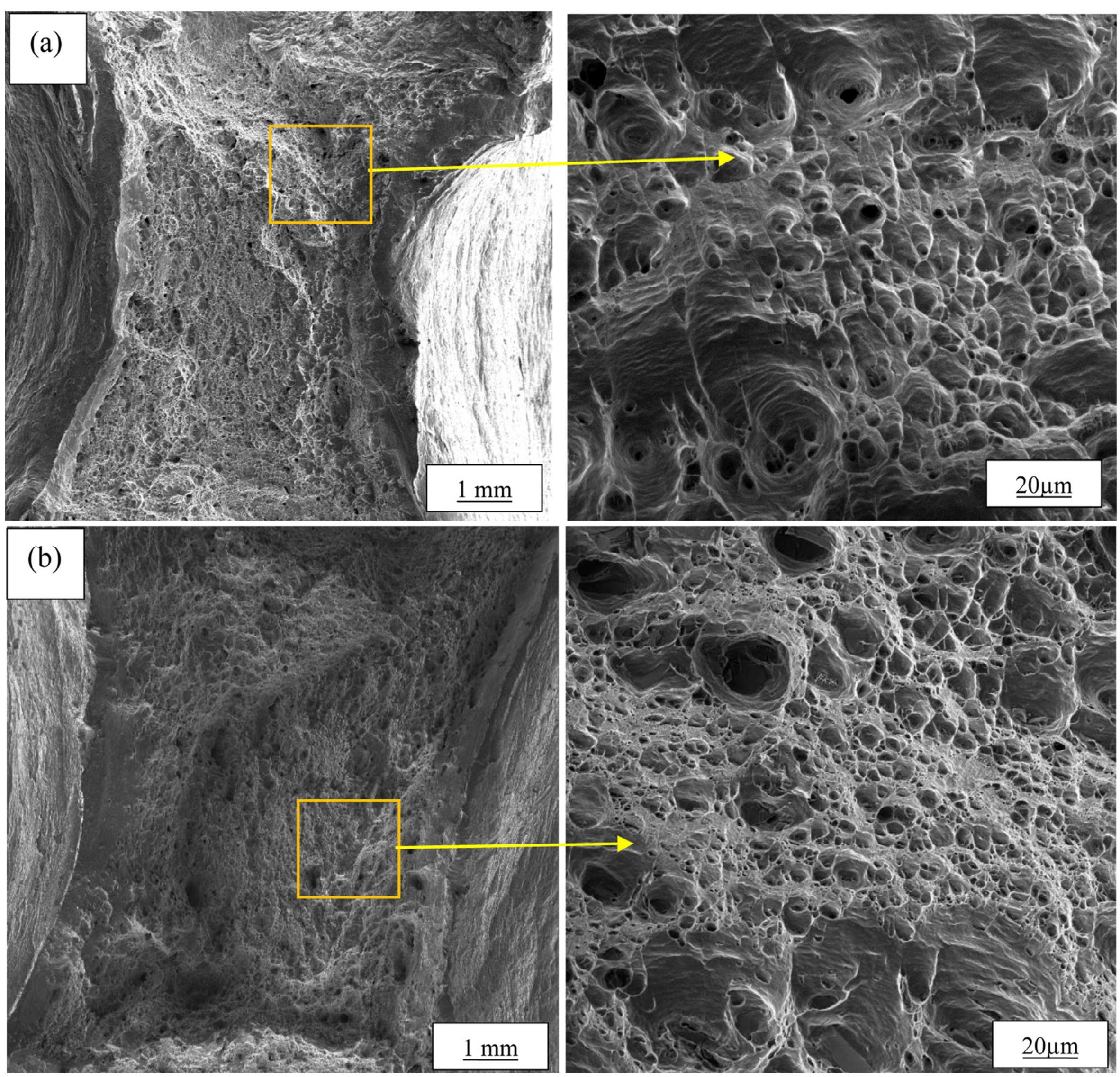

Fig. 4. Multiple-pass SEM fractographs, (a) NFSP, (b) SFSP.

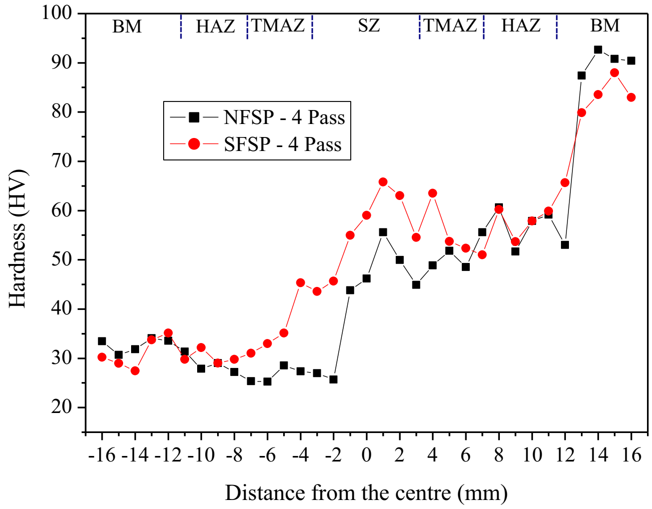

Fig. 5. Hardness profiles.

dynamic recovery, geometric dynamic recrystallization, continuous dynamic recrystallization, and the discontinuous dynamic recrystallization are some of the mechanisms involved during the SFSP [14,16]. Similar findings were reported in the literature, where the submerged multiple passes resulted in finer grain sizes [17,18]. Both joints were found to have significantly refined grain size in comparison to those of the base and single-pass SFSPed and NFSPed joints. The repeated dynamic recrystallization was found to be the technique responsible for the notable microstructural grain refinement during both the multiple-pass NFSP and SFSP [8,19,20].

Fig. 2 shows the tensile stress and strain curves for the multiple-pass NFSP and SFSP joints. Fig. 3 shows the ultimate tensile strength (UTS) and percentage elongation regarding Fig. 2. The multiple-pass NFSP was found to have a UTS of 94.19 MPa and a percentage elongation of 21.95%. The multiple-pass SFSP had a UTS of 97.99 MPa and a percentage elongation of 23.92%. The tensile strength and elongation correspond with the obtained grain sizes. The multiple-pass SFSPed UTS was higher than that of the NFSP joint. This is because the multiple-pass NFSP area experienced repeated over-heating which occurred during the process, resulting in the possible formation of grain growth and material softening [21–23]. It was noted that the multiple-pass SFSP joint had both the highest UTS and percentage elongation, making this joint more ductile than the multiple-pass NFP joint. Similar studies where the application of rapid water cooling resulted in higher UTS and percentage elongation was reported in the literature [13,24].

Fig. 4 shows the SEM fractographs for the multiple-pass NFSP and SFSP. The specimen in both techniques failed on the heat-affected zone of the AA8011 side. Studying the figure it can be seen that the NFSPed joint show the tearing dimples or rather a shearing lip, microvoid coalescence and cleavages. The SFSPed joint is showing similar features but differs in the shape dimples which are more cup or cone-shaped. Based on the mentioned features it can be said that both joints had a ductile fracture [11,25]. The multiple-pass SFSPed fractographs depicted more refined equiaxed dimples, compared to that of the NFSPed one. This behaviour correlates with the grain sizes of the stir zone micrographs. Fig. 5 shows the hardness profiles of the Multiple-pass NFSP and SFSP. The hardness profiles were found to increase to the AA6082 side. This is due to the AA6082 base material having a higher hardness compared to that of the AA8011 base material. The stir zone of the NFSPed joint was found to be approximately 56 HV and 63 HV for the SFSPed joint. The hardness results concur with the grain sizes obtained. The increase in the hardness of the SFSPed joint is a resulted of the rapid cooling which prevented the strengthening precipitates from weakening on the AA6082 alloy [26–29].

4. Conclusions

The multiple-pass normal friction stir processing was successfully analyzed comparatively to the multiple-pass submerged friction stir processing. Based on the results obtained it was discovered that the microstructural grain size of the multiple-pass submerged friction stir processed was 67.72% finer compared to those of the multiple-pass normal friction stir processed joints. The ultimate tensile strength was found to increase with a decrease in grain size, resulting in the multiple-pass submerged joint having a UTS with a 97.99 MPa, whereas the normal friction stir processed joint had a UTS of 94.19 MPa. The percentage elongation results correlated with the tensile and grain size results. The hardness of the multiple-pass submerged friction stir processed joints was found to be 65 HV while the normal friction stir processed joint had a maximum hardness of 53 HV. In summary, the multiple-pass submerged friction stir processing had better results in comparison to the normal friction stir processed ones due to the differences in the heat generated during the processing.

CRediT authorship contribution statement

Sipokazi Mabuwa: Conceptualization, Methodology, Data curation, Writing - original draft, Visualization, Investigation. **Velaphi Msomi:** Supervision, Software, Validation, Writing - review & editing.

Declaration of Competing Interest

The authors declare that they have no known competing financial interests or personal relationships that could have appeared to influence the work reported in this paper.

Acknowledgements

The help and assistance received for the scanning electron microscopy tests from Ms Miranda Waldron from the University Cape Town is greatly acknowledged.

References

[1] Z.Y. Ma, Metall. Mater. Trans. A Phys. Metall. Mater. Sci. 39(2008) 642–658.
[2] R.S. Mishra, Z.Y. Ma, I. Charit, Mater. Sci. Eng. A Struct. Mater. Prop. Microstruct. Process. 341(2003) 307–310.
[3] R.S. Mishra, Z.Y. Ma, Mater. Sci. Eng. R Rep. 50 (2005) 1–78.
[4] N. Sun, D. Apelia, Mater. Sci. Forum. 618–619 (2009) 361–364.
[5] J.Q. Su, T.W. Nelson, Scr. Mater. 52 (2) (2005) 135–140.
[6] S.M. Aktarer, D.M. Sekban, O. Saray, T. Kucukomeroglu, Z.Y. Ma, G. Purcek, Mater. Sci. Eng: A 636 (2015) 311–319.
[7] S.K. Singh, R.J. Immanuel, S. Babu, S.K. Panigrahi, G.D. Janaki Ram, J. Mater. Processing Technol. 236(2016) 252–262.
[8] S. Mabuwa, V. Msomi, Eng. Fail. Anal. 118 (2020) 104876.
[9] S. Mabuwa, V. Msomi, Metals 10 (2020) 1429.
[10] M.V.N.V. Satyanarayana, A. Kumar, J. Phys. Conf. Ser. 1240 (2019) 012077.
[11] S. Mabuwa, V. Msomi, Mater. Res. Express 7 (2020) 096513.
[12] H. Abrams, Metallography 4 (1) (1971) 59–78.
[13] S. Mabuwa, V. Msomi, J. Mater. Res. Techn. 9 (5) (2020) 9632–9644.
[14] A. Eyvazian, A. Hamouda, F. Tarlochan, H.A. Derazkola, F.J. Khodabakhshi, J. Mater. Res. Technol. 9 (3) (2020) 3767–3781.
[15] F. Khodabakhshi, A. Gerlich, A. Simchi, A. Kokabi, Mater. Sci. Eng. 620 (2015) 471–482.
[16] T.R. McNelley, S. Swaminathan, J.Q. Su, Scr. Mater. 58 (5) (2008) 349–354.
[17] F. Chai, D. Zhang, Y. Li, J. Magnes. Alloy 3 (2015) 203–209.
[18] J. Wang, Y. Lu, D. Zhou, Y. Zhang, Z. Bai, X. Li, Mater. Res. Express 6 (2019) 126577.

[19] X.C. Luo, D.T. Zhang, G.H. Cao, C. Qiu, D.L.J. Chen, Mater. Sci. 54 (2019) 8640–8654.
[20] S. Mabuwa, V. Msomi, Mater. Today Proc. (2019), https://doi.org/10.1016/j.matpr.2019.10.039.
[21] R. Prasad, S.P. Tewari, J.K. Singh, Mater. Res. Express. 6 (9) (2019) 096579.
[22] H.A. Derazkola, A. Eyvazian, A. Simchi, Manuf. Process 50 (2020) 68–79.
[23] G. Huang, J. Wu, W. Hou, Y. Shen, Mater. Sci. Eng. A 734 (2018) 353–363.
[24] R. Chandran, S.K.V. Santhanam, Mater. Res. 21:6(2018) e20171070 1–12.
[25] D.C. Hoffman, S.V. Kennesh, Mater. Sci. Eng. A 402 (1–2) (2005) 234–241.
[26] P. Moore, G. Booth, The Welding Engineers Guide to Fracture and Fatigue, Woodhead Publishing, 2015, xvii-xviii. https://doi.org/10.1016/B978-1-78242-370-6.50018-6.
[27] A. Barcellona, G. Buffa, L. Fratini, D. Palmeri, J. Mat. Proc. Techn. 177 (2006) 340–343.
[28] M.D. Sameer, A.K. Birru, J. Magn. Alloy. 7 (2019) 264–271.
[29] P. Cavaliere, A. Squillace, F. Panella, J. Mat. Proc. Techn. 200 (2008) 364–372.